Electrochemistry

International Edition: DOI: 10.1002/anie.201805555
German Edition: DOI: 10.1002/ange.201805555

Identifying the Structural Evolution of the Sodium Ion Battery Na_2FePO_4F Cathode

Qi Li, Zigeng Liu, Feng Zheng, Rui Liu, Jeongjae Lee, Gui-Liang Xu, Guiming Zhong, Xu Hou, Riqiang Fu, Zonghai Chen, Khalil Amine, Jinxiao Mi, Shunqing Wu, Clare P. Grey, and Yong Yang**

Abstract: *Na_2FePO_4F is a promising cathode material for Na-ion batteries owing to its relatively high discharge voltage and excellent cycling performance. Now, the long- and short-range structural evolution of Na_2FePO_4F during cycling is studied by in situ high-energy X-ray diffraction (XRD), ex situ solid-state nuclear magnetic resonance (NMR), and first-principles DFT calculations. DFT calculations suggest that the intermediate phase, $Na_{1.5}FePO_4F$, adopts the space group of $P2_1/c$, which is a subgroup ($P2_1/b11$, No. 14) of Pbcn (No. 60), the space group of the starting phase, Na_2FePO_4F, and this space group provides a good fit to the experimental XRD and NMR results. The two crystallographically unique Na sites in the structure of Na_2FePO_4F behave differently during cycling, where the Na ions on the Na2 site are electrochemically active while those on the Na1 site are inert. This study determines the structural evolution and the electrochemical reaction mechanisms of Na_2FePO_4F in a Na-ion battery.*

The quest for batteries that are low-cost, safe, and environmentally benign to be used in portable devices, electric vehicles, and large-scale energy storage systems continues unabated.[1] While Li-ion batteries (LIBs) provide reliable energy sources for most of the above applications, the limited lithium resources cannot meet the fast growing demand for increasingly larger devices.[2] Therefore, the development of Na-ion batteries (SIBs) has become an alternative strategy, especially in large-scale energy storage systems, owing to the naturally abundant and thus lower cost sodium resources.[3]

To enhance the competitiveness of SIBs, screening cathode materials with high discharge voltages is an important approach. Among the high-voltage candidate cathode materials, polyanionic compounds have attracted great attention owing to their structural diversity and stability. Different types of polyanionic compounds used in SIBs have been reported in the past years, including phosphates, $NaFePO_4$[4] and $Na_3V_2(PO_4)_3$,[5] pyrophosphates, $Na_2MP_2O_7$[6] (M = Fe, Co, Mn), as well as fluorophosphates, Na_2MPO_4F[7] (M = Fe, Co, Mn) and $Na_3V_2O_{2x}(PO_4)_3F_{3-2x}$.[8] These materials have good structural stability but poor electronic conductivity, which can be compensated by carbon coating and/or cation substitution to improve their electrochemical performances.[9]

Among these polyanionic compounds, a layered iron-based fluorophosphate, Na_2FePO_4F, with a space group of *Pbcn*, has been proved to be a promising cathode material for SIBs.[10] Ellis et al. in 2007 reported the extraction of Na ions from Na_2FePO_4F, in a LIB, showing solid-solution-like electrochemical behavior, where transitions between two closely related phases (Na_2FePO_4F to $Na_{1.5}FePO_4F$ and $Na_{1.5}FePO_4F$ to $NaFePO_4F$) were observed and the intermediate phase $Na_{1.5}FePO_4F$, obtained by chemical desodiation, adopted a space group of *P*2/*c*, which is not a subgroup of *Pbcn*.[7a] Recham et al. first published the use of nano-

[*] Q. Li, R. Liu, Dr. G. Zhong, X. Hou, Prof. Y. Yang
State Key Lab of Physical Chemistry of Solid Surfaces, Collaborative Innovation Center of Chemistry for Energy Materials and Department of Chemistry, Xiamen University
Xiamen 361005 (China)
E-mail: yyang@xmu.edu.cn
Dr. Z. Liu, J. Lee, Prof. C. P. Grey
Department of Chemistry, University of Cambridge
Lensfield Rd, Cambridge CB2 1EW (UK)
F. Zheng, Prof. S. Wu
Collaborative Innovation Center for Optoelectronic Semiconductors and Efficient Devices, Department of Physics, Xiamen University
Xiamen 361005 (China)
Dr. G. L. Xu, Dr. Z. Chen, Dr. K. Amine
Chemical Sciences and Engineering Division
Argonne National Laboratory
9700 South Cass Avenue, Argonne, Illinois 60439 (USA)
Dr. K. Amine
Materials Science and Engineering, Stanford University
Stanford, California 94305 (USA)
Dr. G. Zhong
Xiamen Institute of Rare Earth Materials
Chinese Academy of Sciences
Xiamen 361021 (China)
Dr. R. Fu
National High Magnetic Field Laboratory
1800 E. Paul Dirac Drive, Tallahassee, Florida 32310 (USA)
Prof. J. Mi
Department of Material Science and Engineering, Xiamen University
Xiamen 361005 (China)
Dr. Z. Liu
Current address: Max-Plank-Institut für Chemische Energiekonversion
Stiftstr. 34–36, 45470 Mülheim an der Ruhr (Germany)
and
Institut für Energie und Klimaforschung (IEK-9)
Forschungszentrum Jülich GmbH
52425 (Germany)
E-mail: zigeng.liu@cec.mpg.de
zi.liu@fz-juelich.de

Supporting information and the ORCID identification number(s) for the author(s) of this article can be found under: https://doi.org/10.1002/anie.201805555.

Na_2FePO_4F in a SIB with a discharge capacity of 100 mAh g^{-1} in the first cycle.[10c] Deng et al. further improved the cycling performance of carbon-coated Na_2FePO_4F with about 85% capacity retention after 1000 cycles.[10d] Tripathi et al. calculated the migration barriers of Na ions in Na_2FePO_4F, demonstrating high Na mobility between $[FePO_4F]$ layers through a 2D network in the *ac* plane.[11] Recently, Tereshchenko et al. combined XRD and DFT calculations to determine the intermediatephase $Na_{1.55}FePO_4F$ with a space group of $P2_1/b$, and showed that Fe^{II}/Fe^{III} charge ordering was coupled with Na/vacancy ordering.[12] However, Smiley et al. employed ex situ ^{23}Na solid-state nuclear magnetic resonance (ssNMR) to characterize Na_2FePO_4F at different states of charge, showing: a) one single-phase transition between Na_2FePO_4F and $NaFePO_4F$ during the charge process, without detection of intermediate phase $Na_{1.5}FePO_4F$; and b) no evidence of Na ions in a mixed Fe^{II} and Fe^{III} environment,[13] which are in contradiction to other reported results.[7a,12] Thus, the structural evolution and the electrochemical reaction mechanisms of Na_2FePO_4F during the cycling are still under debate.

Herein, we have elucidated the structural evolution and determined how the Na ions in the structure of Na_2FePO_4F (de)intercalate during the cycling through in situ high-energy X-ray diffraction (XRD) patterns, ex situ ssNMR spectra, and first-principles DFT calculations. The results reveal that the whole cycling process of the Na_2FePO_4F cathode is dominated by two two-phase reactions between structures at different states of charge. The intermediate phase, $Na_{1.5}FePO_4F$, with a space group $P2_1/c$, is determined by DFT calculations and agrees with the XRD and ssNMR results. Additionally, we find that the Na ions on the Na2 site are electrochemically active, while the Na ions on the Na1 site are inert and remain in the structure.

Pristine Na_2FePO_4F, synthesized by solid-state methods, crystallized in the space group *Pbcn* (Supporting Information, Figure S1a). As shown in the Supporting Information, Figure S1b, the structure of Na_2FePO_4F comprises $[FePO_4F]$ layers formed by face-sharing FeO_4F_2 octahedra, connected by bridging F atoms and PO_4 tetrahedra. Two different Na sites, as shown in Figure 1a and Figure 1b, are located between the $[FePO_4F]$ layers.[7a] While each Na site has 4 Fe ions in their second coordination shell, the local environment are quite different for these two sites as listed in the Supporting Information, Table S1: a) the Na1 site has two Na–Fe distances of approximately 4.55 Å and two Na–Fe distances around 3.45 Å, while the Na–Fe distances for the Na2 site are all around 3.33 Å; b) the angles of two Na1–F–Fe

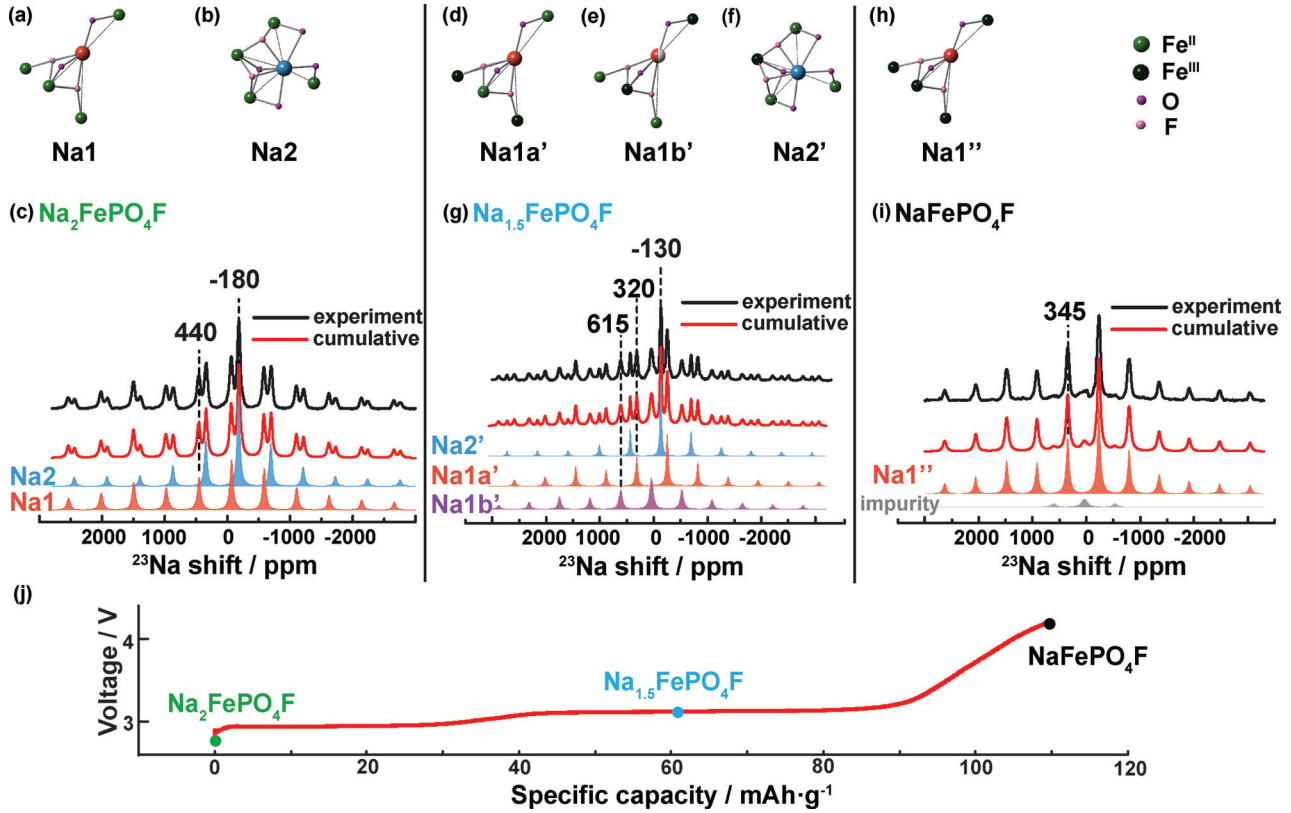

Figure 1. The local environment of the a) Na1 and b) Na2 sites in Na_2FePO_4F. c) ^{23}Na MAS NMR spectrum (black) of Na_2FePO_4F at 55 kHz with the cumulative spectrum (red) and deconvolution of resonances at −180 ppm (light blue) and 440 ppm (light red), respectively. The local environment of the d) Na1a′, e) Na1b′, and f) Na2′ sites in $Na_{1.5}FePO_4F$. g) ^{23}Na MAS NMR spectrum (black) of $Na_{1.5}FePO_4F$ at 60 kHz with the cumulative spectrum (red), deconvolution of resonances at −130 ppm (light blue), 320 ppm (light red) and 615 ppm (purple), respectively. The local environment of the h) Na1″ site in $NaFePO_4F$. i) ^{23}Na MAS NMR spectrum (black) of $NaFePO_4F$ at 60 kHz with the cumulative spectrum (red), deconvolution of resonances at 345 ppm (light red) and around 0 ppm (gray), respectively. The peak around 0 ppm is the diamagnetic impurity. j) The first charge curve of Na_2FePO_4F electrode with corresponding marks for Na_2FePO_4F, $Na_{1.5}FePO_4F$, and $NaFePO_4F$ samples.

bonds are near 180° and other angles of Na1–O/F–Fe bonds are close to 90°, while all the angles of Na2–O/F–Fe bonds are around 90°. In terms of the electron-nuclear dipolar (hyperfine) interaction between the paramagnetic Fe electron and the Na nucleus ($I = 3/2$), this implies a more symmetric interaction tensor for the Na spins on the Na2 site, which has important implications as discussed below.

Since ssNMR is very sensitive to the local environment, two resonances are expected in the ^{23}Na magic angle spinning (MAS) NMR spectrum of Na_2FePO_4F. As shown in the Supporting Information, Figure S1c, two main resonances, the isotropic shifts of which are 440 ppm and −180 ppm at 60 kHz, were observed in the ^{23}Na MAS NMR spectrum of pristine Na_2FePO_4F, along with a weak resonance around 0 ppm, which most likely arose from NaF from the synthesis process. Given that the isotropic peaks and the spinning sidebands are severely overlapped at 60 kHz, a deconvolution (Figure 1c) was performed on a spectrum acquired at 55 kHz. As paramagnetic NMR shifts depend strongly on the sample temperature and frictional MAS heating, all the shifts of isotropic resonances are labeled with those obtained at 60 kHz for consistency. The intensity ratio between the two resonances at 440 and −180 ppm is about 1.04:0.96, which is in reasonable agreement with the 1:1 occupancy ratio between the two Na sites in the structure.

Furthermore, comparing the two resonances, we observe more symmetric sideband manifolds that span a narrower range for the resonance at −180 ppm. In contrast, the resonance at 440 ppm shows asymmetric sideband manifolds in which the spinning sidebands positioned at −62 ppm and −572 ppm have even stronger signal intensity than the isotropic resonance (Supporting Information, Figure S1d). Considering that the major contribution to the sideband manifolds of the two Na resonances is the electron–nuclear dipolar interaction between Na and Fe ions,[14] we tentatively assign the resonances at −180 ppm and 440 ppm to the Na2 and Na1 site, respectively.

However, accurate characterization of spinning sideband manifolds in paramagnetic NMR can be difficult due to bulk magnetic susceptibility of powders; this is further complicated by the possible interplay between the interaction between the electron–nuclear hyperfine tensor and quadrupolar tensor.[15] Hence, first-principles DFT calculations were also employed to estimate the isotropic shifts of the two Na sites in Na_2FePO_4F. Detailed information from the DFT calculations are shown in the Supporting Information. The contour maps of electron spin density around the two Na sites in Na_2FePO_4F obtained from projected DFT wave functions are shown in the Supporting Information, Figure S5, where the spin density with opposite sign is transferred to the two Na sites, resulting in positive and negative shifts for the Na1 and Na2 resonances, respectively, in the ^{23}Na MAS NMR spectra. The calculated isotropic shifts δ_{iso} and the asymmetry parameter κ are in agreement with our experimental results, which lie between the Hyb20 and Hyb35 calculated values listed in Table 1. However, our results contradict with the previous assignment by Smiley et al.,[13] where the resonance at 450 ppm with broader sideband manifolds was assigned to the Na2 site, and the resonance at −175 ppm with narrower sideband manifolds was assigned to the Na1 site. It is possible that the complexity of this material and the multiple overlapping spinning sidebands, combined with the aforementioned difficulties in characterizing the sideband manifolds, resulted in the different assignment.

The electrochemical performance of the Na_2FePO_4F cathode in a Na-ion battery (Supporting Information, Figure S6) clearly reveals two two-phase processes and the formation of an intermediate phase $Na_{1.5}FePO_4F$ at current rates from 0.1 C to 1 C. Considering this intermediate phase, we have generated numerous possible configurations for the intermediate phase $Na_{1.5}FePO_4F$ by extracting half of the Na ions from the Na2 site in the Na_2FePO_4F unit cell; DFT calculations were then performed on each configuration, optimizing each structure, and ranking the energies of the different structures. The XRD patterns generated from possible configurations which have different Na vacancies are shown in the Supporting Information, Figure S2a, and the experimental XRD pattern of electrochemically prepared $Na_{1.5}FePO_4F$ matches the lowest-energy phase, indexed as $P2_1/c$, which is quite different with the previous reported space group of $P2/c$ (No. 13) reported by Ellis et al.,[7a] owing to their different crystallographic setting, but it agrees with that determined by Tereshchenko et al.[12] Detailed information concerning the proposed configurations and Rietveld refinement are shown in the Supporting Information. $P2_1/c$ is a subgroup ($P2_1/b11$, No. 14) of $Pbcn$ (No. 60), the space group observed for the starting material Na_2FePO_4F, resulting from a symmetry reduction arising from the loss of orthogonality between the b- and c-axis in Na_2FePO_4F. Note that the earlier reported space group of $P2/c$ for $Na_{1.5}FePO_4F$ is not a subgroup of $Pbcn$ (subgroup of $Pbcn$ is $P2/a$ related to its setting).[7a] Bond valence sum (BVS in valence unit or vu)

Table 1: DFT calculated and experimental ^{23}Na shifts of Na_xFePO_4F ($x = 2$, 1.5, and 1).

	Na site	DFT Hyb20[a]			DFT Hyb35[a]			Expt	Smiley et al.[13]
		δ_{iso} [ppm]	Ω[b] [ppm]	κ[b]	δ_{iso} [ppm]	Ω[b] [ppm]	κ[b]	δ_{iso} [ppm]	δ_{iso} [ppm]
Na_2FePO_4F	Na1	528	367933	−0.81	387	375951	−0.81	440	−175
	Na2	−187	189983	−0.19	−227	195953	−0.19	−180	450
$Na_{1.5}FePO_4F$	Na1a′	445	435543	−0.90	224	438015	−0.92	320	–
	Na1b′	628	428220	−0.78	516	435808	−0.75	615	–
	Na2′	−209	200183	−0.35	−307	192689	−0.42	−130	–
$NaFePO_4F$	Na1″	505	494692	−0.90	263	507725	−0.90	345	350

[a] Hyb20 and Hyb35 refers to the proportion of Hartree–Fock exchange energy in the hybrid calculation. [b] Ω gives the span of anisotropy and κ gives the asymmetry.

calculations[16] listed in the Supporting Information, Table S4, suggest that Fe1 and Fe2 correspond to Fe^{II} and Fe^{III} ions, respectively. Therefore, an additional Na1 site and an extra Fe site are obtained in this lowest-energy phase of $Na_{1.5}FePO_4F$, resulting in different Fe ion configurations in the second coordination shell of the two Na1 sites, labeled as Na1a′ and Na1b′ in Figure 1d and Figure 1e. Thus, the six bonds (Supporting Information, Table S5) connecting Na1 to Fe via O/F are further divided to two classes: a) 4 bonds with the distances between Na1a′ to Fe^{II} being less than 4 Å and angles nearing 90° while other 2 bonds with the distances between Na1a′ to Fe^{III} nearing 4.5 Å and angles nearing 180°; b) 4 bonds with the distances between Na1b′ to Fe^{III} being less than 4 Å and angles nearing 90° while other 2 bonds with the distances between Na1b′ to Fe^{II} being nearing 4.5 Å and angles nearing 180°, which implies different paramagnetic shifts of the Na1a′ and Na1b′ sites in $Na_{1.5}FePO_4F$ we will discuss below.

The almost identical ^{23}Na MAS NMR spectra of $Na_{1.5}FePO_4F$ prepared by chemical and electrochemical desodiation are shown in the Supporting Information, Figure S3a, indicating the same final product for both processes. Figure 1g shows the deconvolution spectra of electrochemically prepared $Na_{1.5}FePO_4F$ with three isotropic resonances located at 615, 320, and −130 ppm. According to the local environment of the Na sites mentioned above and the Hyb20 and Hyb35 calculated values listed in Table 1, these three resonances at 615, 320, and −130 ppm are assigned to the Na1b′, Na1a′, and Na2′ sites, respectively. DFT predictions of the shifts of the other configurations of $Na_{1.5}FePO_4F$ (Supporting Information, Table S7) do not agree with these shifts, further confirming the existence of this phase. Of note, our DFT and NMR results show no vacancy on Na1a′ and Na1b′ sites and there is only one site for Na2′, while the result from Tereshchenko et al. show that there is 9% vacancy on the second Na1 sites, and around 18% Na partially occupied the second Na2 sites in $Na_{1.55}FePO_4F$. The difference of the Na occupancy most likely arises from the process of refining the light atom Na in XRD patterns, resulting in a better fitting but a slight mismatch for the real occupancy distribution.

Now moving to $NaFePO_4F$, with all the Fe^{II} oxidized to Fe^{III}. This gives four Fe^{III} ions in the second coordination shell of the Na1″ site (Figure 1h), and the space group returns to *Pbcn*. Such higher symmetry arises from all the Fe and Na sites being identical again, which also manifests in a single isotropic ^{23}Na resonance at 345 ppm of both electrochemically and chemically prepared $NaFePO_4F$ (Supporting Information, Figure S3b). This resonance is assigned to the Na1″ site in $NaFePO_4F$, which is in agreement with our DFT calculation results and also with the previous assignment by Smiley et al.[13]

To investigate the structural evolution of cathode Na_2FePO_4F further, ex situ ssNMR was employed to characterize samples prepared at different states of charge, with their corresponding amount of Na remaining in the structure listed in the Supporting Information, Tables S8 and S9. To deconvolute the severely overlapped isotropic resonances from the spinning sidebands, again, two spectra at 60 kHz and 55 kHz were measured.

In the charge process (Figure 2a–c), from pristine, Na_2FePO_4F, to C6, $Na_{1.5}FePO_4F$, the Na1 resonance gradually decreases, while the resonances at 615 ppm (Na1b′), and 320 ppm (Na1a′), start to appear and gradually increase, with the total amount of these three resonances remaining constant. Meanwhile, the Na2 resonance gradually decreases until completely disappearing at C6, while another resonance at −130 ppm (Na2′) appears and gradually increases. The intensity of the Na2′ resonance in sample C6 is half of the intensity of Na2 resonance in pristine sample, meaning half the Na ions on the Na2 site are deintercalated in this process. These observations imply a two-phase reaction process from pristine to C6, which agrees with our electrochemical measurements and in situ HEXRD results in the Supporting Information.

From C6, $Na_{1.5}FePO_4F$, to C8, $NaFePO_4F$, Na1a′ and Na1b′ resonances decrease then disappear, while a new resonance at 345 ppm (Na1″) appears and gradually increases. Additionally, the intensity of the Na1″ resonance in sample C8 is almost equal to that of the Na1 resonance of pristine Na_2FePO_4F as well as the sum of the Na1a′ and Na1b′ resonances in sample C6. The Na2′ resonance decreases until disappearing at C8, indicating the Na ions on the Na2′ site are totally extracted at the end of charge.

The discharge process (Figure 2d–f) shows reversible behavior as compared to the charge process, which indicates Na_2FePO_4F shows highly reversible capacity when used as a cathode for a SIB. Indeed, Deng et al. has demonstrated the excellent cycling performance of Na_2FePO_4F with about 85% capacity retention after 1000 cycles.[10d]

In summary, the whole cycling process of Na_2FePO_4F consists of two two-phase reactions between three structures at different states of charge: Na_2FePO_4F, $Na_{1.5}FePO_4F$, and $NaFePO_4F$ with space group of *Pbcn*, $P2_1/c$, and *Pbcn*, respectively. The structure of the intermediate phase, $Na_{1.5}FePO_4F$, is identified by DFT calculations and confirmed via a comparison between the experimental ^{23}Na NMR spectra as well as hyperfine shifts calculated via hybrid-DFT calculations. Na1 remains in the structure while Na2 (de)intercalates from/into the structure along the cycling. This work provides in-depth analysis of the structural evolution and the electrochemical reaction mechanisms of cathode Na_2FePO_4F for a SIB.

Acknowledgements

This work was supported by the National Natural Science Foundation of China (Grant No. 21233004, 21761132030, and 21621091) and the National Basic Research Program of China (Grant No. 2016YFB0901502 and 2018YFB0905400). This research used resources of the Center for Functional Nanomaterials, which is a U.S. DOE Office of Science User Facility, at Brookhaven National Laboratory under Contract No. DE-SC0012704. Research at Argonne National Laboratory is supported by the U.S. Department of Energy (DOE), Vehicle Technologies Office. Argonne National Laboratory is operated for DOE Office of Science by UChicago Argonne, LLC, under contract number DE-AC02-06CH11357. The authors

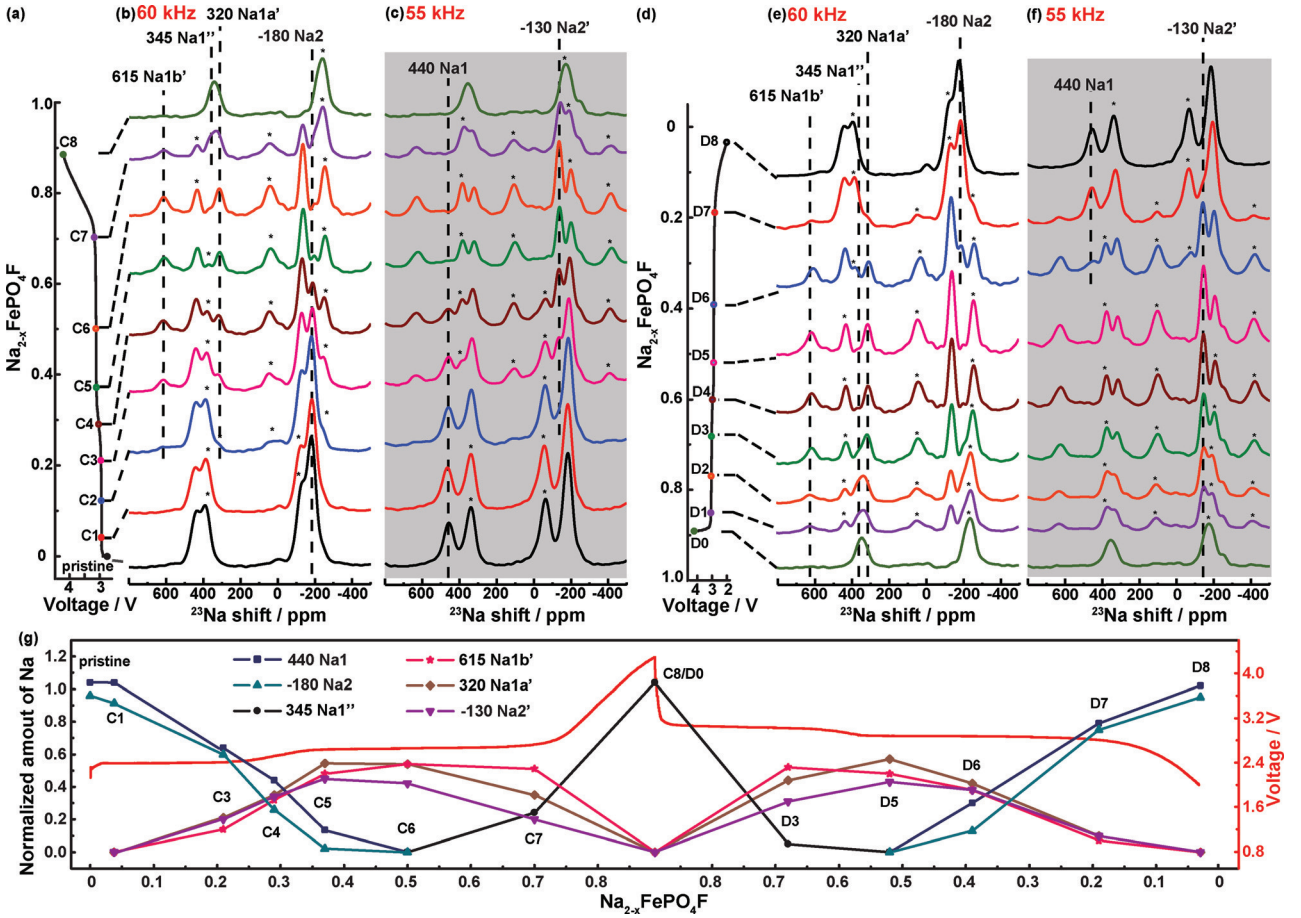

Figure 2. a) Selected different states of charge and the normalized ^{23}Na MAS NMR spectra of Na_2FePO_4F during first charge process at b) 60 kHz and c) 55 kHz, respectively. d) Selected different states of charge and the normalized ^{23}Na MAS NMR spectra of Na_2FePO_4F during first discharge process at e) 60 kHz and f) 55 kHz, respectively. Spinning sidebands are marked with an asterisk (*). g) The distribution of Na ions on different Na sites during first cycle with the electrochemical profile shown as red solid line.

also thank the support from Clean Vehicles—US–China Clean Energy Research Center (CERC-CVC2). R.F. also wishes to acknowledge support from the National High Magnetic Field Laboratory (NHMFL), which is supported by the NSF Cooperative Agreement No. DMR-1644779 and the State of Florida.

Conflict of interest

The authors declare no conflict of interest.

Keywords: density functional calculations · electrochemistry · Na_2FePO_4F · NMR spectroscopy · sodium-ion batteries

How to cite: *Angew. Chem. Int. Ed.* **2018**, *57*, 11918–11923
Angew. Chem. **2018**, *130*, 12094–12099

[1] a) P. G. Bruce, B. Scrosati, J.-M. Tarascon, *Angew. Chem. Int. Ed.* **2008**, *47*, 2930–2946; *Angew. Chem.* **2008**, *120*, 2972–2989; b) J. B. Goodenough, K.-S. Park, *J. Am. Chem. Soc.* **2013**, *135*, 1167–1176; c) M. Armand, J.-M. Tarascon, *Nature* **2008**, *451*, 652–657.

[2] M. D. Slater, D. Kim, E. Lee, C. S. Johnson, *Adv. Funct. Mater.* **2013**, *23*, 947–958.

[3] a) N. Yabuuchi, K. Kubota, M. Dahbi, S. Komaba, *Chem. Rev.* **2014**, *114*, 11636–11682; b) D. Kundu, E. Talaie, V. Duffort, L. F. Nazar, *Angew. Chem. Int. Ed.* **2015**, *54*, 3431–3448; *Angew. Chem.* **2015**, *127*, 3495–3513; c) H. Pan, Y.-S. Hu, L. Chen, *Energy Environ. Sci.* **2013**, *6*, 2338–2360.

[4] M. Casas-Cabanas, V. V. Roddatis, D. Saurel, P. Kubiak, J. Carretero-González, V. Palomares, P. Serras, T. Rojo, *J. Mater. Chem.* **2012**, *22*, 17421–17423.

[5] Z. Jian, C. Yuan, W. Han, X. Lu, L. Gu, X. Xi, Y. S. Hu, H. Li, W. Chen, D. Chen, *Adv. Funct. Mater.* **2014**, *24*, 4265–4272.

[6] a) P. Barpanda, T. Ye, S.-i. Nishimura, S.-C. Chung, Y. Yamada, M. Okubo, H. Zhou, A. Yamada, *Electrochem. Commun.* **2012**, *24*, 116–119; b) P. Barpanda, T. Ye, M. Avdeev, S.-C. Chung, A. Yamada, *J. Mater. Chem. A* **2013**, *1*, 4194–4197; c) P. Barpanda, J. Lu, T. Ye, M. Kajiyama, S.-C. Chung, N. Yabuuchi, S. Komaba, A. Yamada, *RSC Adv.* **2013**, *3*, 3857–3860.

[7] a) B. Ellis, W. Makahnouk, Y. Makimura, K. Toghill, L. Nazar, *Nat. Mater.* **2007**, *6*, 749–753; b) X. Wu, J. Zheng, Z. Gong, Y. Yang, *J. Mater. Chem.* **2011**, *21*, 18630–18637; c) B. L. Ellis, W. M. Makahnouk, W. Rowan-Weetaluktuk, D. Ryan, L. F. Nazar, *Chem. Mater.* **2010**, *22*, 1059–1070.

[8] a) P. Serras, V. Palomares, A. Goñi, I. G. de Muro, P. Kubiak, L. Lezama, T. Rojo, *J. Mater. Chem.* **2012**, *22*, 22301–22308; b) Z. Liu, Y.-Y. Hu, M. T. Dunstan, H. Huo, X. Hao, H. Zou, G. Zhong, Y. Yang, C. P. Grey, *Chem. Mater.* **2014**, *26*, 2513–2521.

[9] a) S. Li, Y. Dong, L. Xu, X. Xu, L. He, L. Mai, *Adv. Mater.* **2014**, *26*, 3545–3553; b) C. Zhu, K. Song, P. A. van Aken, J. Maier, Y.

Yu, *Nano Lett.* **2014**, *14*, 2175 – 2180; c) M. Aragón, P. Lavela, G. Ortiz, J. Tirado, *J. Electrochem. Soc.* **2015**, *162*, A3077 – A3083.
[10] a) Y. Kawabe, N. Yabuuchi, M. Kajiyama, N. Fukuhara, T. Inamasu, R. Okuyama, I. Nakai, S. Komaba, *Electrochem. Commun.* **2011**, *13*, 1225 – 1228; b) A. Langrock, Y. Xu, Y. Liu, S. Ehrman, A. Manivannan, C. Wang, *J. Power Sources* **2013**, *223*, 62 – 67; c) N. Recham, J.-N. Chotard, L. Dupont, K. Djellab, M. Armand, J.-M. Tarascon, *J. Electrochem. Soc.* **2009**, *156*, A993 – A999; d) X. Deng, W. Shi, J. Sunarso, M. Liu, Z. Shao, *ACS Appl. Mater. Interfaces* **2017**, *9*, 16280 – 16287.
[11] R. Tripathi, S. M. Wood, M. S. Islam, L. F. Nazar, *Energy Environ. Sci.* **2013**, *6*, 2257 – 2264.
[12] I. V. Tereshchenko, D. A. Aksyonov, O. A. Drozhzhin, I. A. Presniakov, A. V. Sobolev, A. Zhugayevych, D. Striukov, K. J. Stevenson, E. Antipov, A. M. Abakumov, *J. Am. Chem. Soc.* **2018**, *140*, 3994 – 4003.
[13] D. L. Smiley, G. R. Goward, *Chem. Mater.* **2016**, *28*, 7645 – 7656.
[14] C. P. Grey, N. Dupré, *Chem. Rev.* **2004**, *104*, 4493 – 4512.
[15] a) C. P. Grey, C. M. Dobson, A. K. Cheetham, *J. Magn. Reson.* **1992**, *98*, 414 – 420; b) J. Lee, I. D. Seymour, A. J. Pell, S. E. Dutton, C. P. Grey, *Phys. Chem. Chem. Phys.* **2017**, *19*, 613 – 625.
[16] N. E. Brese, M. O'Keeffe, *Acta Crystallogr. Sect. B* **1991**, *47*, 192 – 197.

Manuscript received: May 14, 2018
Revised manuscript received: July 16, 2018
Accepted manuscript online: July 24, 2018
Version of record online: August 19, 2018

